

Rethinking Boundary Discontinuity Problem for Oriented Object Detection

Hang Xu^{1,2*} Xinyuan Liu^{2,3*} Haonan Xu^{2,3}
Yike Ma² Zunjie Zhu^{1,4} Chenggang Yan^{1,4} Feng Dai^{2†}

¹Hangzhou Dianzi University, Hangzhou, China

²Institute of Computing Technology, Chinese Academy of Sciences, Beijing, China

³University of Chinese Academy of Sciences, Beijing, China

⁴Lishui Institute of Hangzhou Dianzi University, Lishui, China

Abstract

Oriented object detection has been developed rapidly in the past few years, where rotation equivariant is crucial for detectors to predict rotated bounding boxes. It is expected that the prediction can maintain the corresponding rotation when objects rotate, but severe mutational in angular prediction is sometimes observed when objects rotate near the boundary angle, which is well-known boundary discontinuity problem. The problem has been long believed to be caused by the sharp loss increase at the angular boundary during training, and widely used IoU-like loss generally deal with this problem by loss-smoothing. However, we experimentally find that even state-of-the-art IoU-like methods do not actually solve the problem. On further analysis, we find the essential cause of the problem lies at discontinuous angular ground-truth(box), not just discontinuous loss. There always exists an irreparable gap between continuous model output and discontinuous angular ground-truth, so angular prediction near the breakpoints becomes highly unstable, which cannot be eliminated just by loss-smoothing in IoU-like methods. To thoroughly solve this problem, we propose a simple and effective Angle Correct Module (ACM) based on polar coordinate decomposition. ACM can be easily plugged into the workflow of oriented object detectors to repair angular prediction. It converts the smooth value of the model output into sawtooth angular value, and then IoU-like loss can fully release their potential. Extensive experiments on multiple datasets show that whether Gaussian-based or SkewIoU methods are improved to the same performance of AP₅₀ and AP₇₅ with the enhancement of ACM.

1 Introduction

As an expansion of horizontal object detection [1–3], oriented object detection has a wider range of applications in many scenes, such as aerial images [4, 5], panoramic images [6, 7], scene text [8], 3D objects [9], etc, since it can achieve a good balance between fine localization and low labeling cost. In oriented object detection, a detector need predict the minimal enclosing rotated rectangle bounding boxes for objects, so it has a high requirement for rotation equivariant. The concept refers to the ability of the detector to predict the correct bounding box angles regardless of the object’s orientation. However, researchers have observed mutation in angular prediction when objects rotate near the boundary angle, which is commonly known as boundary discontinuity problem [10, 11].

*Equal contribution.

†Feng Dai (fdai@ict.ac.cn) is the corresponding author.

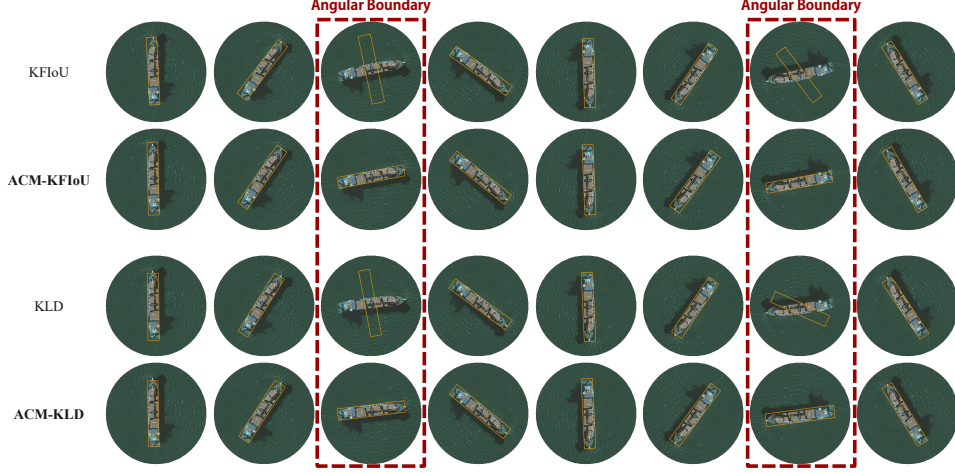


Figure 1: When objects rotate near the boundary angle, state-of-the-art IoU-like methods (e.g., KFIOU [16], KLD [14]) actually suffer from severe mutational in angular prediction. With the correction for angle by proposed ACM, the prediction truly achieves rotation equivariant.

In previous works, the boundary discontinuity problem has been long believed to be caused by the sharp loss increase at the angular boundary during training. To address this problem, researchers designed a series of smooth loss functions to prevent the sharp loss increase, and these methods can be divided into two categories, i.e., separate-optimization loss [10, 12, 13] and joint-optimization loss (dominant by IoU-like loss) [14, 11, 15, 16]. Due to the negative impact of the low consistency between loss and IoU-metric, the detectors trained through the separate-optimization loss are usually worse than IoU-like loss. It has long been a consensus in object detection [17–19], so more and more IoU-like loss methods become mainstream choices for training oriented object detectors.

However, we experimentally find that even state-of-the-art IoU-like methods do not actually solve the boundary discontinuity problem. Specifically, we select an image containing only a single object, and rotate it 360° at 1° intervals to obtain a series of images. These images are sequentially fed into a well-trained detector (with state-of-the-art IoU-like methods) for inference. As is shown in Figure 1, visualized results show that the predicted boxes can tightly enclose object in most cases, but collapse with a seriously deviated angle in some case near the angular boundary.

Through theoretical analysis, we find that the essential cause of the boundary discontinuity problem lies at discontinuous angular ground-truth(box), not just discontinuous loss. Since the detector actually predict box properties from the input object image, it need to fit the relationship between box and object. Counterintuitively, object and box are essentially distinct concepts with rotation period 2π and π respectively, which causes the relationship between angle of box and object become sawtooth wave containing breakpoints, as is shown in Figure 2. The discontinuous angle is actually hard to fit directly, and relying on loss-smoothing alone is not sufficient to overcome this difficulty. There always exists an irreparable gap between continuous model output and discontinuous angular ground-truth, so angular prediction near the breakpoints becomes highly unstable, which is the ultimate truth about boundary discontinuity problem.

To thoroughly solve this problem, detectors should output truly sawtooth wave angles, like ground-truth angles, rather than continuous values. To this end, we propose a simple and effective Angle Correct Module (ACM) based on polar coordinate decomposition. As is shown in Figure 3, ACM can be easily plugged into the existing workflow of oriented object detectors to repair angular prediction. It converts the smooth value of the model output into sawtooth angular value, which eliminate the instability of angular prediction caused by breakpoint issue, so those IoU-like loss can be better used to optimize the box parameters. Finally, boundary discontinuity problem is solves thoroughly, as is shown in Figure 1. **Overall, our contribution can be summarized as following:**

- We analyse the essential cause of the boundary discontinuity problem in oriented object detection, i.e., an irreparable gap between continuous model output and discontinuous angular ground-truth, which cannot be eliminated just by loss-smoothing in IoU-like methods.

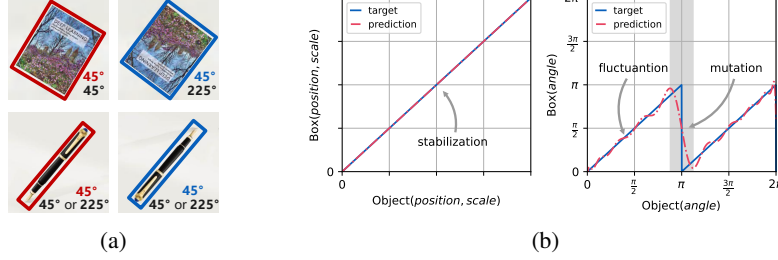


Figure 2: Object instance and Bounding box are different concepts: (a) objects rotated with 45° and 225° [black mark] share the same box rotated with 45° [colorful mark], which causes (b) the relationship [blue line] between *angle* of box and object become sawtooth wave containing a breakpoint [gray region], differing from the (*position, scale*). Not only is the prediction [red line] of the breakpoint region mutational, but the prediction [red line] of other regions also becomes fluctuant.

- We propose a simple and effective Angle Correct Module (ACM). ACM can be easily plugged into the workflow of oriented object detectors to address the boundary discontinuity problem, so that the IoU-like loss can be better used to optimize detectors.
- Extensive experiments on multiple datasets show that whether Gaussian-based or SkewIoU methods are improved to the same performance of AP_{50} and AP_{75} with the enhancement of ACM.

2 Problem Analysis

2.1 Related Works

In oriented detection, the minimal enclosing rotated bounding box (x, y, w, h, θ) is adopted widely to represent an oriented object, where (x, y) is center position, (w, h) is scale (i.e., weight & height) and θ is rotated angle of box. There are many algorithms inherited from classic horizontal detection to predict the rotated boxes, where ROI-Transformer [4], SCRDet [20], ReDet [21] are two-stage mainstreamed methods, while DRN [22], R³Det [23], S²A-Net [24] are single-stage methods. However, these methods suffer from boundary discontinuity problem in varying degrees. In previous works, the problem always blames to the sharp loss increase at the angular boundary during training, so researchers always attempt to solve the problem by smoothing loss at the angular boundary. CSL [10] designs a circular smooth label loss to classify angle, DCL [12] utilizes dense code to accelerate CSL, and GF-CSL [25] adopts a dynamic weights to stabilize CSL. MGAR [26] introduces a multi-grained angular mechanism to refine orientation, and PSC [13] introduces phase-shifting encoding for accurate orientation. These methods realize loss-smoothing, but such separate-optimization is usually weaker than IoU-like joint-optimization since the latter has higher consistency with IoU-metric. It has long been a consensus in object detection [17–19], so more and more IoU-like loss functions become mainstream choices for training oriented object detectors. IoU-Smooth L1 [20] utilizes IoU guide Smooth L1 in magnitude, and RIoU [9] utilizes projection operator to estimate IoU. GWD [11] and KLD [14] transform rotated box into smooth Gaussian distribution, and then measure distribution distance to keep consistency with IoU. KFIoU [16] also adopts Gaussian modeling but directly approximate the calculation of IoU. SkewIoU [15] derives the formula of IoU between rotated rectangles, but it is rarely used in researches due to its complexity. These IoU-like loss functions help the model to achieve SOTA results, but we find the boundary problem has not been really solved in practice. In the following, we will illustrate the essential cause of the boundary problem lies at discontinuous angular ground-truth, not just discontinuous loss.

2.2 Essential Cause of the Boundary Discontinuity Problem

For an oriented object detector, it accepts images of objects as input, and outputs bounding boxes with *position, scale* and *angle* parameters. However, we reveal that object and box are essentially different concepts, which will produce breakpoints in the angular ground-truth. The discontinuous ground-truth cannot be fitted exactly by continuous output of the detector especially at the breakpoints, so angular prediction near the breakpoints become very unstable, which causes the boundary issue.

For convenience, we denote the object and box as $O(position, scale, angle)$ and $B(position, scale, angle)$, respectively. The difference between O and B lie in *angle* rather than *position* and *scale*, where the range of O_{angle} is $[0, 2\pi)$ while the range of B_{angle} is $[0, \pi)$. This is because the object hold content which needs to rotate at least one full circle to be completely overlapped, while the box is a kind of geometry without any content which just needs to rotate half of circle to be completely overlapped. For example in Figure 2a, objects rotated with 45° and 225° can be distinguished by content, while the corresponding bounding boxes cannot as well. Furthermore, there are deeper considerations behind the adoption of representing object with a nature-distinct box. On the one hand, in order to avoid confuse the detector during training, the box angle of objects need to be unified in annotation. Continuing with Figure 2a as example, we can easily determine which book is 45° and which book is 225° , but the same thing is hard for the pen due to the lack of consensus about 0° orientation of the pen. On the other hand, in practice people never care if the detected object is upright or inverted. For example, all boxes in Figure 2a are acceptable, and 45° or 225° cannot affect the Average Precision (AP) derived from the IoU during evaluating the model.

In this setting, the bounding box is a truly symmetric rectangle, whose rotations θ and $\theta \pm \pi$ are indistinguishable. As a result, the relationship between B_{angle} and O_{angle} exhibits a **sawtooth wave**, rather than a straight line for the relationship between $(B_{position}, B_{scale})$ and $(O_{position}, O_{scale})$, as is shown in Equation 1 and corresponding image (blue solid line) in Figure 2b.

$$\begin{cases} B_{position} = O_{position} \\ B_{scale} = O_{scale} \\ B_{angle} = O_{angle} \bmod \pi \end{cases} \quad (1)$$

The detector takes the object image as input and the bounding box as supervision, which means that the detector is actually enforced to fit Equation 1 (blue solid lines in Figure 2b). Obviously, B_{angle} has a jump at $O_{angle} = \pi$, which makes it difficult for the detector F , a **continuous function essentially**, to fit it accurately. There always exists a small interval $(\pi - \epsilon_1, \pi + \epsilon_2)$ near the breakpoint (gray region in Figure 2b), where predicted angle (red dash line) drops rapidly from π to 0, and angular prediction becomes highly unstable, resulting in a severe degradation of the AP/IoU of boxes. In addition, angular prediction even outside the interval becomes a bit fluctuant.

Although existing IoU-like joint-optimization loss functions used to claim to solve boundary discontinuity problem, we observe that, compared to the \ln -norm loss, they actually just smooth out the losses in the angular boundary, rather than smooth out the angle itself. It means that angle as a discontinuous value is still hard to fit directly, and boundary problem is still not addressed.

3 Method

3.1 Motivation

Based on the above analysis, we believe that the migration from loss-smoothing to angle-smoothing will become the key to solving the boundary problem. To this end, it is necessary to first figure out how previous methods achieve loss-smoothing. For convenience, let the ground-truth and prediction of B_{angle} be denoted as θ_t and θ_p , respectively. The way to optimize angle in previous methods can be reformulated as follows:

$$\theta = \arg \min_{\theta_p} \mathcal{L}_{f,\ell}(\theta_p; \theta_t) = \arg \min_{\theta_p} \ell(f(\theta_p); f(\theta_t)) \quad (2)$$

where model fits discontinuous θ_p , f and ℓ are the wrapping function for angle and measuring function for wrapped value, respectively. For example, **1**) in the case of joint-optimization for angle using KLD, $f = gaussian_{x,y,w,h}(\theta)$, $\ell = \ell_{kld}$. f wraps the angle and other parameters as a smooth Gaussian distribution, and ℓ just measures the distance of Gaussian distribution between prediction and ground-truth; **2**) in the case of joint-optimization for angle using SkewIoU, f and ℓ are implicit functions derived from $SkewIoU(\theta_p^{xywh}, \theta_t^{xywh})$. Although we cannot get explicit expression of f and ℓ , their role must be similar to $gaussian_{x,y,w,h}(\theta)$ and ℓ_{kld} .

To summary up, the key to loss-smoothing is to convert discontinuous value into smooth value. Such being the case, it is a better choice to make model directly fit the smooth value rather than utilize it just in loss calculation, which will no longer exceed the ability of the model to fit. Then we can

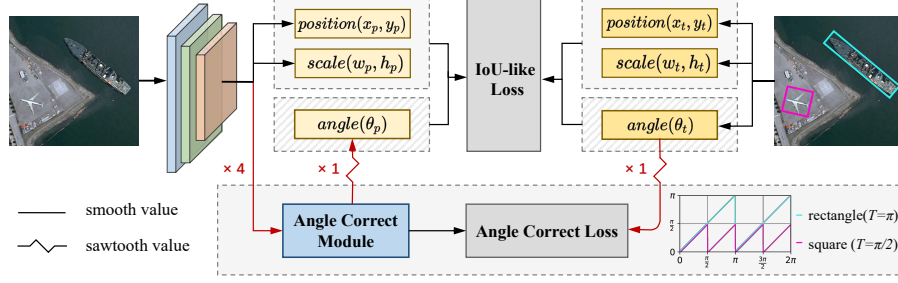


Figure 3: Overview of proposed Angle Correct Module (ACM). The detector fits **4-dimensional** continuous, differentiable and reversible wrapped values ($f_x^{(2)}, f_y^{(2)}, f_x^{(4)}, f_y^{(4)}$), and ACM converts them to **1-dimensional** sawtoothed angle (θ_p). Finally, the corrected angle is used to calculate IoU-like loss, which eliminates boundary problem thoroughly.

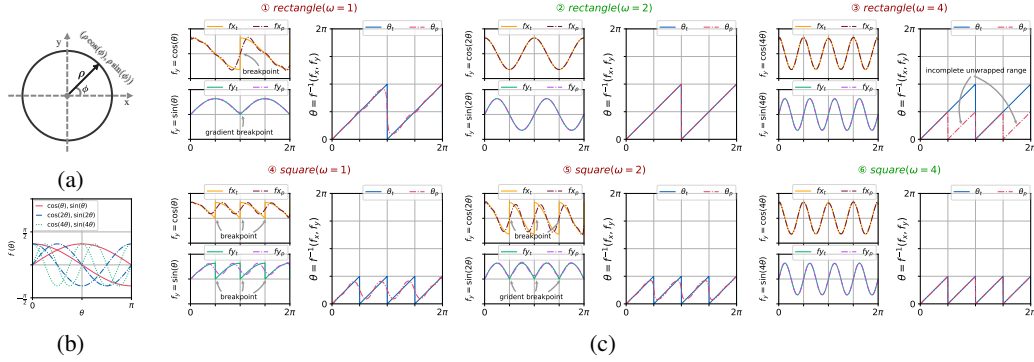


Figure 4: Based on (a) polar coordinate decomposition, we define (b) a 2-dimensional wrapping function $f(\theta)$. It will (c) compound onto the original sawtooth wave $\theta = B_{angle}(O_{angle})$, and exhibits different effect for rectangular (top, $T = \pi$) & square-like (bottom, $T = \frac{\pi}{2}$) objects when angular frequency $\omega = 1, 2, 4$. **The target and prediction are marked as solid line and dash line, respectively.** The optimal angular frequency for rectangular & square-like objects is 2 and 4, respectively.

get discontinuous angle by the inverse transform for the smooth value. In this case, the optimization formula of angle can be rewrite as follows:

$$\theta^* = f^{-1}(\arg \min_{f_p} \mathcal{L}_{f, \ell}(f_p; \theta_t)) = f^{-1}(\arg \min_{f_p} \ell(f_p; f(\theta_t))) \quad (3)$$

where model fits continuous f_p , f^{-1} is the inverse function of f , and we can get angle by $\theta_p = f^{-1}(f_p)$. Compared with θ , θ^* will no longer suffer from difficulty about fitting breakpoints.

Obviously, f need to satisfy reversibility in addition to smoothness (i.e., continuity and differentiability), which is not available in f of previous methods [14, 11, 16, 15]. To this end, we propose a **Angle Correct Module (ACM)** based on polar coordinate decomposition. The module implements the above f , which can be easily plugged into the existing workflow of oriented object detectors to repair angular prediction. As is shown in Figure 3, ACM converts the smooth value of the model output into sawtooth angular value, and eliminate the instability of angle prediction due to breakpoint issue.

3.2 Angle Correct Module (ACM)

To implement a truly available detection algorithm based on wrapped angle prediction, we must find a continuous, differentiable, and reversible function f . Since $\theta = B_{angle}(O_{angle}) \in [0, \pi)$, $f(\theta)$ just needs to be defined on $[0, \pi)$. To eliminate the breakpoint at $O_{angle} = \pi$, we need to ensure that $f(B_{angle}(\pi^-)) = f(B_{angle}(\pi^+))$, which is equivalent to $f(\pi) = f(0)$. However, it directly violates the necessary condition for functional injectivity. Due to the requirement about continuity of f , it also causes a many-to-one correspondences not only at the interval boundary but also at other points, making it impossible for the detector to unwrap single unique angle value in the inference phase.

To eliminate this ambiguity, we extend f from a one-dimensional scalar function to a two-dimensional vector function, and get inspired by polar coordinate decomposition. As is shown in Figure 4a, given a vector with polar angle ϕ and radius(length) ρ in 2-dimensional space, it can be decompose as $(\rho \cos(\phi), \rho \sin(\phi))$ in Cartesian coordinates. When the radius ρ is fixed and ϕ is just considered in single period, the polar angle and Cartesian coordinates are one-to-one correspondences. Therefore, we can use this relationship to design f and obtain the corresponding f^{-1} as & Figure 4b:

$$(f_x, f_y) = f(\theta) = (\cos(\omega\theta), \sin(\omega\theta)) \quad (4)$$

$$\theta^{(\omega)} = f^{-1}(f_x, f_y) = \frac{1}{\omega}((\arctan2(f_y, f_x) + 2\pi) \bmod 2\pi) \quad (5)$$

where $\omega \in R^+$ is angular frequency, $\arctan2$ is another version of \arctan with quadrant assignment, and f_x, f_y is the components of $f(\theta)$ in two dimensions, and $\theta^{(\omega)}$ is unwrapped angle from f_x, f_y .

Although the single dimensional $\cos(\omega\theta)$ and $\sin(\omega\theta)$ are many-to-one, integration of them can achieve a one-to-one effect in a higher dimension, making f an reversible transformation. Due to polar coordinate unwrapping can get unique angle only in a single cycle, $\omega\theta$'s range $[0, \omega\pi) \subseteq [0, 2\pi)$, so it is necessary to satisfy $\omega \leq 2$. In conjunction with ground-truth(solid lines) in Figure 4c(top), we further discuss this range as follows.

- When $\omega = 2$, f_x and f_y are both smooth (continuous and with continuous gradient) at $O_{angle} = \pi$, and the problem of breakpoint is well-solved.
- When $\omega = 1$, f_x has a breakpoint at $O_{angle} = \pi$, while f_y is not differentiable at $O_{angle} = \pi$ although it is continuous (such gradient breakpoint maybe hinders model optimization).
- When $\omega \neq 2$ and $\omega \neq 1$, both f_x and f_y have breakpoint at $O_{angle} = \pi$.

By comparing prediction(dash lines) with ground-truth(solid lines) in Figure 4c(top), we can find once ground-truth of wrapped value contains breakpoints, its prediction will become significantly worse, and according unwrapped angle, too. **Finally, only $\omega = 2$ is the optimal choice that makes f continuous, differentiable, and reversible for rectangular objects.**

3.3 Extension to Square-like Object

When the value of the object's width and height are close to each other, the bounding box will become a square-like from rectangle, which possesses stronger symmetry and leads to the period of B_{angle} shrinking from π to $\frac{\pi}{2}$. As a result, breakpoints will occur at more locations (i.e., $\frac{\pi}{2}, \pi$, and $\frac{3\pi}{2}$). In this case, if we continue to use Angle Correct Module proposed in the previous section, we should set ω to 4 accordingly, as is shown in Figure 4c(bottom). It is worth noting that when $\omega = 2$, breakpoints still exist in f_x at $O_{angle} = \frac{\pi}{2}, \pi, \frac{3\pi}{2}$, while f_y suffers from gradient breakpoints at these positions although it is continuous, which is similar to the case of $\omega = 1$ for the rectangle.

3.4 Generalization for Objects with Varied Aspect Ratio

Considering that the actual scene contains both square-like and rectangular objects, we attempt to use wrapped values with two frequencies (denoted as $f^{(\omega)}$, where $\omega = 2, 4$) simultaneously and fuse the unwrapped results to obtain a more accurate angular prediction. For boxes rotated within $[0, \frac{\pi}{2})$, both $f^{(2)}$ and $f^{(4)}$ can unwrap correct angles. For boxes rotated within $[\frac{\pi}{2}, \pi)$, $f^{(2)}$ still unwraps correctly, while $f^{(4)}$'s unwrapped angles will be offset by one decoding-period $\frac{\pi}{2}$ to fall in $[0, \frac{\pi}{2})$. Therefore, ideally the difference between $\theta^{(2)} \in [0, \pi)$ and $\theta^{(4)} \in [0, \frac{\pi}{2})$ could only be 0 or $\frac{\pi}{2}$, but it only affects rectangle ($T = \pi$) and not square-like ($T = \frac{\pi}{2}$) in both training and inference phase. Note that $f^{(2)}$ suffers from breakpoints only for square-like rather than rectangle, and $f^{(4)}$ is immune to breakpoints for both rectangle and square-like, which just fails to correctly determine period range belonging to angles. Thus we can utilize coarse $\theta^{(2)}$ to correct the period range of fine $\theta^{(4)}$ as follows, where relaxation condition outside the parentheses are adopted in practice due to the independent errors of $f^{(2)}$ & $f^{(4)}$. **Finally, we use this fusion strategy to adapt objects with varied aspect ratio.**

$$\theta = \begin{cases} \theta^{(4)} + \frac{\pi}{2} & , \text{if } \theta^{(2)} - \theta^{(4)} > \frac{\pi}{4} \quad (\theta^{(2)} - \theta^{(4)} = \frac{\pi}{2}) \\ \theta^{(4)} & , \text{if } \theta^{(2)} - \theta^{(4)} \leq \frac{\pi}{4} \quad (\theta^{(2)} = \theta^{(4)}) \end{cases} \quad (6)$$

3.5 Loss Functions

As is shown in Figure 3, given a batch of images, the detector outputs the classification c_p , position (x_p, y_p) , scale (w_p, h_p) , and warped angle f_p^θ , and the corresponding ground truth is c_t , (x_t, y_t) , (w_t, h_t) , and θ_t . First, we calculate the direct loss of the wrapped angle in Angle Correct Module(ACM), named as **Angle Correct Loss(ACL)**, which is

$$\mathcal{L}_{acm} = \ell_{smooth_l1}(f_p^\theta, f(\theta_t)) \quad (7)$$

Then, we jointly optimize the unwrapped f_p^θ , i.e., θ_p , with (x_p, y_p) , (w_p, h_p) , which is

$$\mathcal{L}_{box} = \ell(B(x_p, y_p, w_p, h_p, f^{-1}(f_p^\theta)), B(x_t, y_t, w_t, h_t, \theta_t)) \quad (8)$$

where $\ell \in \{\ell_{riou}, \ell_{kld}, \ell_{gwd}, \dots\}$. In addition, we also calculate the classification loss, which is

$$\mathcal{L}_{cls} = \ell_{focal}(c_p, c_t) \quad (9)$$

Finally, the total loss is as follows (λ_{box} , λ_{acm} are coefficients to balance each parts of loss):

$$\mathcal{L} = \mathcal{L}_{cls} + \lambda_{box}\mathcal{L}_{box} + \lambda_{acm}\mathcal{L}_{acm} \quad (10)$$

By default, we set $\lambda_{box} = 1$, $\lambda_{acm} = 0.2$ in experiments.

4 Experiment

4.1 Datasets and Implementation Details

HRSC2016 [27] contains images from two scenarios with ships on sea and close inshore. The training, validation and testing set include 436, 181 and 444 images, with the image size ranging from 300×300 to 1500×900 . We adjust the long side of each image to a fixed size (640 pixels) and keep the original aspect ratio for training and testing.

UCAS-AOD [28] contains two categories: Car and Plane, which includes 1,510 aerial images of about $659 \times 1,280$ pixels, with two categories of 14,596 instances in total. We randomly select 1,110 for training and 400 for testing. Finally, we adopt the same data processing strategy as HRSC2016.

DOTA [29] is one of the largest datasets for oriented object detection in aerial images, which contains 2,806 images, with fifteen categories of 188,282 instances in total. The training, validation and testing set include 1411, 458 and 937 images, respectively. The categories are defined as: Plane (PL), Baseball Diamond (BD), Bridge (BR), Ground Field Track (GTF), Small Vehicle (SV), Large Vehicle (LV), Ship (SH), Tennis Court (TC), Basketball Court (BC), Storage Tank (ST), Soccer-Ball Field (SBF), Roundabout (RA), Harbor (HA), Swimming Pool (SP), and Helicopter (HC). To fit the limited GPU memory, we crop training images into the patches of size 1024×1024 pixels with an overlap of 256 pixels. Thus, there are 16,853 labeled images during the training stage. In testing stage, we crop the testing set images into 4000×4000 patches with an overlap of 1024 pixels to mitigate the impact of detection errors at the cutting edge.

Evaluation Metric. Methods are evaluated using the standard COCO style Average Precision (AP) [30], which is the convention throughout the field of object detection. It is worth noting that AP_{75} is gradually replacing AP_{50} as the most reliable metric for oriented object detection due to AP_{75} 's higher sensitivity to angle deviation than AP_{50} . Following mainstream works [14, 31], we adopt AP_{75} as main metric, while AP_{50} is auxiliary metric.

Implementation Details. All approaches are implemented in PyTorch, and training is done on GeForce RTX 3090 GPUs. We choose the anchor-free method CenterNet [32] to build the rotated detector and ImageNet pretrained ResNet-50 [33] as the backbone. The whole network is optimized by Adam for 140 epochs with the learning rate dropped by $10\times$ at 100 and 130 epochs. As the DOTA dataset takes a relatively large image resolution (1024×1024) as an input, the batch size is set as 12 with an initial learning rate 1.25×10^{-4} . For the HRSC2016 and UCAS-AOD datasets, the batch size is set as 32, and the initial learning rates are set as 2×10^{-4} and 1×10^{-4} , respectively.

4.2 Ablation Study

To verify the effectiveness of the proposed the ACM module, we design the following ablation study. We use the state-of-the-art KFIoU [16] loss as the baseline in ablation study.

Table 1: Ablation experiments of ACM with different angular frequencies.

$\omega = 1$	$\omega = 2$	$\omega = 4$	HRSC2016		DOTA	
			AP ₅₀	AP ₇₅	AP ₅₀	AP ₇₅
✓	✓	✓	88.26	62.95	71.97	26.11
			90.44 (+2.18)	78.90 (+15.95)	73.51 (+1.54)	39.29 (+13.18)
			90.58 (+2.32)	86.12 (+23.17)	73.08 (+1.11)	39.62 (+13.51)
			24.90 (-63.36)	20.82 (-42.13)	35.50 (-36.47)	17.29 (-8.82)
	✓	✓	90.55 (+2.29)	87.77 (+24.82)	74.51 (+2.54)	40.49 (+14.38)

Table 2: Ablation experiments of Angle Correct Loss(ACL).

ACM	ACL	HRSC2016		DOTA	
		AP ₅₀	AP ₇₅	AP ₅₀	AP ₇₅
✓	✓	88.26	62.95	71.97	26.11
		37.37 (-50.89)	13.98 (-48.97)	54.67 (-17.3)	19.67 (-6.44)
		90.55 (+2.29)	87.77 (+24.82)	73.08 (+1.11)	40.49 (+14.38)

Table 3: AP of different objects on HRSC2016 and UCAS-AOD.

Method	HRSC2016 (Ship)		UCAS-AOD (Car)		UCAS-AOD (Plane)	
	AP ₅₀	AP ₇₅	AP ₅₀	AP ₇₅	AP ₅₀	AP ₇₅
GWD [11]	84.94	61.87	87.25	28.46	90.34	38.22
ACM-GWD	90.63 (+5.69)	86.71 (+24.84)	88.69 (+1.44)	29.15 (+0.69)	90.35 (+0.01)	76.00 (+37.78)
KLD [14]	90.01	79.29	87.54	29.99	90.33	29.19
ACM-KLD	90.55 (+0.54)	87.45 (+8.16)	88.76 (+1.22)	30.40 (+0.41)	90.39 (+0.06)	75.65 (+46.46)
KFIoU [16]	88.26	62.95	85.74	24.44	90.34	16.81
ACM-KFIoU	90.55 (+2.29)	87.77 (+24.82)	88.31 (+2.57)	34.81 (+10.37)	90.40 (+0.06)	74.48 (+57.67)
SkewIoU [15]	89.39	76.43	87.73	27.59	90.34	63.64
ACM-SkewIoU	90.47 (+1.08)	88.33 (+11.09)	88.27 (+0.54)	29.13 (+1.74)	90.37 (+0.03)	75.13 (+11.49)

Ablation study of ACM with different angular frequencies. As mentioned in Section 3.2, it is crucial to choose a suitable angular frequencies in ACM. To verify our analysis, we conducted experiments with angular frequencies ($\omega = 1, 2, 4$), as is shown in Table 1. Compared with original KFIoU [16], enhanced version with ACM($\omega = 1$) get remarkable improvement since sinusoidal component in decomposition of the angle has no breakpoints for rectangles. Moreover, ACM($\omega = 2$) eliminates all breakpoints in both two components in decomposition of the angle for rectangles, so it achieves greater improvement. Due to the inability to unwrap the full angular range for rectangles, ACM($\omega = 4$) exhibits severe performance degradation, especially for HRSC2016 dataset consisting entirely of large aspect ratio ships. When adopted the fusion of two angular frequencies simultaneously ($\omega = 2, 4$), compared to $\omega = 2$, the results have little effect on large aspect ratios objects on HRSC2016 dataset and the results have slightly improved on DOTA dataset. This is because the DOTA dataset contains both large aspect ratio objects and square-like objects. Overall, AP (especially AP₇₅) can benefit a lot from ACM, which verifies our analysis. In following experiments, we adopt mixed angular frequencies ($\omega = 2, 4$).

Ablation study of Angle Correct Loss. To verify the necessity of Angle Correct Loss(ACL), we conduct experiments with/without ACL. As is shown in Table 2, plugging ACM alone without ACL supervision for wrapped angles can severely hurt detection performance. As mentioned in Section 3.2, ACM has strict requirements for frequency, and it always unwraps angles under preset frequencies($\omega = 2, 4$). However, it is difficult to ensure that predicted frequencies align with the preset if without direct supervision, and such mismatch will make unwrapped angles fall into a wrong range, so performance degenerates. By the way, since the size of DOTA dataset is much larger than HRSC2016 dataset, the mismatch can get some mitigation, but just like a drop in the ocean.

4.3 Evaluations

Baseline Methods. To verify the generality of our methods, we compare the performance of detectors based on four state-of-the-art IoU-like loss functions, including distribution-based GWD [11] & KLD [14], and geometry-based KFIoU [16] & SkewIoU [15]. To make it fair, we keep all the experiments settings and hyper parameters the same as depicted in corresponding papers.

Quantitative Results on HRSC2016 and UCAS-AOD. The HRSC2016 dataset contains large aspect ratio ships, and the UCAS-AOD dataset contains rectangle cars and square-like planes. Obviously, such pure datasets allow us to focus on the specific cases. As is shown in Table 3, both AP₅₀ and AP₇₅ get significant improvement from ACM on HRSC2016(Ship) and UCAS-AOD(Car). It is worth noting that the improvement of AP₅₀ are negligible on the UCAS-AOD(Plane) dataset, while the improvement of AP₇₅ are tremendous. It is never an accident, and the reasons include: **1)** For square-like objects, the IoU is always over 0.5 regardless of the angle of the predicted box, making AP₅₀ insensitive to square-like objects. **2)** When a square-like box is converted to a 2D-Gaussian distribution, the 2D-Gaussian distribution is completely symmetric like a circle, which makes it

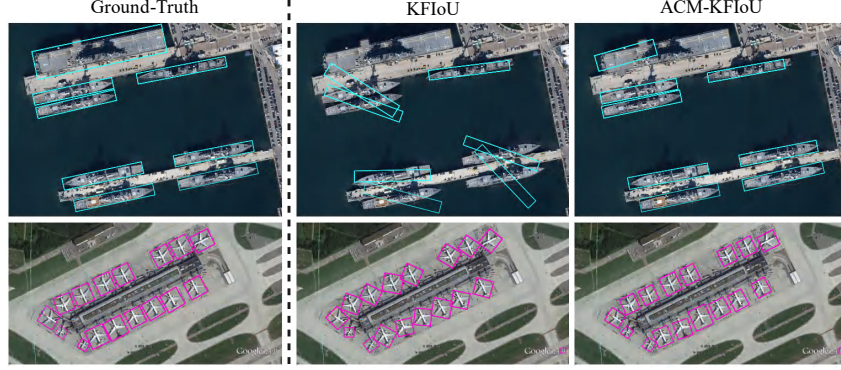


Figure 5: Visualized comparison of detection results between KFIoU [16] and enhanced ACM-KFIoU. The top images are large aspect ratio ships on HRSC2016 dataset and the bottom images are square-like planes on UCAS-AOD dataset.

Table 4: AP of different objects on DOTA.

Method	PL	BD	BR	GTF	SV	LV	SH	TC	BC	ST	SBF	RA	HA	SP	HC	AP ₅₀	AP ₇₅	AP ₅₀₋₉₅
GWD [11]	89.67	78.96	44.88	62.18	78.08	79.74	86.77	90.65	78.58	84.23	54.39	63.96	68.13	73.85	62.7	73.12	34.98	39.15
ACM-GWD	89.55	76.43	51.41	66.2	78.96	79.66	87.57	90.86	80.97	84.2	54.98	61.17	75.34	71.3	57.08	73.71	41.97 (+6.99)	42.81
KLD [14]	89.77	79.42	48.73	67.94	76.96	78.89	87.02	90.79	78.98	82.06	51.45	57.98	72.28	70.87	68.09	73.41	35.25	39.65
ACM-KLD	89.69	76.92	51.54	70.07	78.15	80.07	87.34	90.89	79.64	82.39	50.95	64.27	75.52	72.74	59.04	73.95	42.97 (+7.72)	42.88
KFIoU [16]	89.50	76.89	46.06	64.41	78.39	79.22	86.36	90.75	78.24	82.81	48.97	60.12	66.17	68.83	62.63	71.97	26.11	35.11
ACM-KFIoU	89.68	79.19	48.75	68.77	78.55	80.96	87.54	90.88	79.69	82.6	53.35	63.87	76.04	72.91	64.85	74.51	40.49 (+14.38)	42.45
SkewIoU [15]	89.75	76.29	50.18	67.19	78.33	79.98	87.02	90.55	79.7	82.82	53.45	60.19	72.74	72.24	63.82	73.62	38.01	40.56
ACM-SkewIoU	89.76	79.95	51.75	66.41	78.55	80.37	87.9	90.85	79.13	83.38	52.35	60.89	75.82	73.34	62.71	74.21	42.83 (+4.37)	42.74

impossible for these methods (GWD, KLD, KFIoU) based on 2D-Gaussian distribution to accurately predict the angle of square-like objects. Since our ACM is friendly to square-like objects, it greatly improves these baseline methods based on 2D-Gaussian distribution by **37.78%** (GWD), **46.46%** (KLD) and **57.56%** (KFIoU) on AP₇₅ on UCAS-AOD(Plane) dataset.

We visualize some of the predicted results shown in Figure 5. From the results, we can observe that ACM-KFIoU can predict the angle more accurately than the original KFIoU, both for large aspect ratio ships on HRSC2016 dataset and square-like planes on UCAS-AOD dataset. The visualization results are consistent with the data results in Table 3.

Quantitative Results on DOTA. DOTA dataset contains a considerable number of categories and complexity scenes. Experimental results at Table 4 shows that the performance of all IoU-like methods are improved by **6.99%** (GWD), **7.72%** (KLD), **14.34%** (KFIoU) and **14.34%** (SkewIoU) on AP₇₅ after the ACM module is used. We also unexpectedly find that after the ACM module enhancement, both Gaussian-based loss and SkewIoU loss become very close in terms of AP₅₀ (**73.71%**, **73.95%**, **74.51%**, **74.21%**) and AP₇₅ (**41.97%**, **42.97%**, **40.49%**, **42.83%**), indicating that the primary distinction between them lies in their optimization capabilities for the boundary discontinuity of angle.

5 Discussions

Limitation. Our method cannot be directly applied to quadrilateral detection without angle [34].

Potential societal impacts. Our research may be applied to some sensitive fields, such as remote sensing, aviation, and unmanned aerial vehicles.

Conclusion. In this paper, we experimentally find that widely used IoU-like methods do not actually solve the well-known boundary discontinuity problem. On further analysis, we find the essential cause of the problem lies at discontinuous angular ground-truth(box), not just discontinuous loss. With the help of our proposed Angle Correct Module (ACM) based on polar coordinate decomposition, the smooth value of the model output is converted into sawtooth angular value, and then IoU-like methods can fully release their potential. Extensive quantitative & qualitative experiments show that our methods eliminates boundary problem thoroughly.

References

- [1] Shaoqing Ren, Kaiming He, Ross Girshick, and Jian Sun. Faster r-cnn: Towards real-time object detection with region proposal networks. In *Advances in Neural Information Processing Systems*, pages 91–99, 2015.
- [2] Tsung-Yi Lin, Piotr Dollár, Ross Girshick, Kaiming He, Bharath Hariharan, and Serge Belongie. Feature pyramid networks for object detection. In *Proceedings of the IEEE Conference on Computer Vision and Pattern Recognition*, pages 2117–2125, 2017.
- [3] Tsung-Yi Lin, Priya Goyal, Ross Girshick, Kaiming He, and Piotr Dollár. Focal loss for dense object detection. In *Proceedings of the IEEE International Conference on Computer Vision*, pages 2980–2988, 2017.
- [4] Jian Ding, Nan Xue, Yang Long, Gui-Song Xia, and Qikai Lu. Learning roi transformer for oriented object detection in aerial images. In *Proceedings of the IEEE Conference on Computer Vision and Pattern Recognition*, pages 2849–2858, 2019.
- [5] Yongchao Xu, Mingtao Fu, Qimeng Wang, Yukang Wang, Kai Chen, Gui-Song Xia, and Xiang Bai. Gliding vertex on the horizontal bounding box for multi-oriented object detection. *IEEE Transactions on Pattern Analysis and Machine Intelligence*, 43(4):1452–1459, 2020.
- [6] Hang Xu, Qiang Zhao, Yike Ma, Xiaodong Li, Peng Yuan, Bailan Feng, Chenggang Yan, and Feng Dai. Pandora: A panoramic detection dataset for object with orientation. In *European Conference on Computer Vision (ECCV)*, pages 237–252, 2022.
- [7] Xinyuan Liu, Hang Xu, Bin Chen, Qiang Zhao, Yike Ma, Chenggang Yan, and Feng Dai. Sph2pob: Boosting object detection on spherical images with planar oriented boxes methods. In *International Joint Conference on Artificial Intelligence (IJCAI)*, 2023.
- [8] Yingying Jiang, Xiangyu Zhu, Xiaobing Wang, Shuli Yang, Wei Li, Hua Wang, Pei Fu, and Zhenbo Luo. R2cnn: rotational region cnn for orientation robust scene text detection. *arXiv preprint arXiv:1706.09579*, 2017.
- [9] Yu Zheng, Danyang Zhang, Sinan Xie, Jiwen Lu, and Jie Zhou. Rotation-robust intersection over union for 3d object detection. In *European Conference on Computer Vision*, pages 464–480. Springer, 2020.
- [10] Xue Yang and Junchi Yan. Arbitrary-oriented object detection with circular smooth label. In *European Conference on Computer Vision*, pages 677–694. Springer, 2020.
- [11] Xue Yang, Junchi Yan, Qi Ming, Wentao Wang, Xiaopeng Zhang, and Qi Tian. Rethinking rotated object detection with gaussian wasserstein distance loss. In *International Conference on Machine Learning*, pages 11830–11841. PMLR, 2021.
- [12] Xue Yang, Liping Hou, Yue Zhou, Wentao Wang, and Junchi Yan. Dense label encoding for boundary discontinuity free rotation detection. In *Proceedings of the IEEE Conference on Computer Vision and Pattern Recognition*, pages 15819–15829, 2021.
- [13] Yi Yu and Feipeng Da. Phase-shifting coder: Predicting accurate orientation in oriented object detection. In *IEEE/CVF Conference on Computer Vision and Pattern Recognition*, 2023.
- [14] Xue Yang, Xiaojiang Yang, Jirui Yang, Qi Ming, Wentao Wang, Qi Tian, and Junchi Yan. Learning high-precision bounding box for rotated object detection via kullback-leibler divergence. *Advances in Neural Information Processing Systems*, 34, 2021.
- [15] Dingfu Zhou, Jin Fang, Xibin Song, Chenye Guan, Junbo Yin, Yuchao Dai, and Ruigang Yang. Iou loss for 2d/3d object detection. In *2019 International Conference on 3D Vision*, pages 85–94. IEEE, 2019.
- [16] Xue Yang, Yue Zhou, Gefan Zhang, Jirui Yang, Wentao Wang, Junchi Yan, Xiaopeng Zhang, and Qi Tian. The kfiou loss for rotated object detection. In *International Conference on Learning Representations*, 2023.

- [17] Jiahui Yu, Yuning Jiang, Zhangyang Wang, Zhimin Cao, and Thomas Huang. Unitbox: An advanced object detection network. In *Proceedings of the 24th ACM international conference on Multimedia*, pages 516–520, 2016.
- [18] Hamid Rezatofighi, Nathan Tsoi, JunYoung Gwak, Amir Sadeghian, Ian Reid, and Silvio Savarese. Generalized intersection over union: A metric and a loss for bounding box regression. In *Proceedings of the IEEE Conference on Computer Vision and Pattern Recognition*, pages 658–666, 2019.
- [19] Zhaohui Zheng, Ping Wang, Wei Liu, Jinze Li, Rongguang Ye, and Dongwei Ren. Distance-iou loss: Faster and better learning for bounding box regression. In *Proceedings of the AAAI Conference on Artificial Intelligence*, pages 12993–13000, 2020.
- [20] Xue Yang, Jirui Yang, Junchi Yan, Yue Zhang, Tengfei Zhang, Zhi Guo, Xian Sun, and Kun Fu. Scrnet: Towards more robust detection for small, cluttered and rotated objects. In *Proceedings of the IEEE International Conference on Computer Vision*, pages 8232–8241, 2019.
- [21] Jiaming Han, Jian Ding, Nan Xue, and Gui-Song Xia. Redet: A rotation-equivariant detector for aerial object detection. In *Proceedings of the IEEE Conference on Computer Vision and Pattern Recognition*, pages 2786–2795, 2021.
- [22] Xingjia Pan, Yuqiang Ren, Kekai Sheng, Weiming Dong, Haolei Yuan, Xiaowei Guo, Chongyang Ma, and Changsheng Xu. Dynamic refinement network for oriented and densely packed object detection. In *Proceedings of the IEEE Conference on Computer Vision and Pattern Recognition*, pages 11207–11216, 2020.
- [23] Xue Yang, Junchi Yan, Ziming Feng, and Tao He. R3det: Refined single-stage detector with feature refinement for rotating object. In *Proceedings of the AAAI Conference on Artificial Intelligence*, volume 35, pages 3163–3171, 2021.
- [24] Jiaming Han, Jian Ding, Jie Li, and Gui-Song Xia. Align deep features for oriented object detection. *IEEE Transactions on Geoscience and Remote Sensing*, 2021.
- [25] Jian Wang, Fan Li, and Haixia Bi. Gaussian focal loss: Learning distribution polarized angle prediction for rotated object detection in aerial images. *IEEE Transactions on Geoscience and Remote Sensing*, 60:1–13, 2022.
- [26] Hao Wang, Zhanchao Huang, Zhengchao Chen, Ying Song, and Wei Li. Multigrained angle representation for remote-sensing object detection. *IEEE Transactions on Geoscience and Remote Sensing*, 60:1–13, 2022.
- [27] Zikun Liu, Liu Yuan, Lubin Weng, and Yiping Yang. A high resolution optical satellite image dataset for ship recognition and some new baselines. In *Proceedings of the International Conference on Pattern Recognition Applications and Methods*, volume 2, pages 324–331, 2017.
- [28] Haigang Zhu, Xiaogang Chen, Weiqun Dai, Kun Fu, Qixiang Ye, and Jianbin Jiao. Orientation robust object detection in aerial images using deep convolutional neural network. In *2015 IEEE International Conference on Image Processing*, pages 3735–3739. IEEE, 2015.
- [29] Gui-Song Xia, Xiang Bai, Jian Ding, Zhen Zhu, Serge Belongie, Jiebo Luo, Mihai Datcu, Marcello Pelillo, and Liangpei Zhang. DOTA: A large-scale dataset for object detection in aerial images. In *Proceedings of the IEEE Conference on Computer Vision and Pattern Recognition*, pages 3974–3983, 2018.
- [30] Tsung-Yi Lin, Michael Maire, Serge Belongie, James Hays, Pietro Perona, Deva Ramanan, Piotr Dollár, and C Lawrence Zitnick. Microsoft coco: Common objects in context. In *European Conference on Computer Vision*, pages 740–755. Springer, 2014.
- [31] Ying Zeng, Xue Yang, Qingyun Li, Yushi Chen, and Junchi Yan. Ars-detr: Aspect ratio sensitive oriented object detection with transformer. *arXiv preprint arXiv:2303.04989*, 2023.
- [32] Xingyi Zhou, Dequan Wang, and Philipp Krähenbühl. Objects as points. *arXiv preprint arXiv:1904.07850*, 2019.

- [33] Kaiming He, Xiangyu Zhang, Shaoqing Ren, and Jian Sun. Deep residual learning for image recognition. In *Proceedings of the IEEE Conference on Computer Vision and Pattern Recognition*, pages 770–778, 2016.
- [34] Wen Qian, Xue Yang, Silong Peng, Junchi Yan, and Yue Guo. Learning modulated loss for rotated object detection. In *Proceedings of the AAAI Conference on Artificial Intelligence*, volume 35, pages 2458–2466, 2021.